Optimisation of Nuclear Data Experiments using OpenMC Simulation of a Hyper Pure Germanium Detector

A dissertation submitted to the University of Manchester for the degree of Masters of Science in Nuclear Science and Technology in the Faculty of Science and Engineering

2024

11477108

Alex Leung

Faculty of Science and Engineering

Department of Physics and Astronomy

Declaration

No portion of the work referred to in the thesis has been submitted in support of an application for another degree or qualification of this or any other university or other institute of learning.

Copyright Statement

Abstract

The demand of more accurate nuclear data such as reaction cross sections is crucial in many industries within the field of science and engineering, but the experimental process of measuring these nuclear properties are traditionally not optimial. Optimising nuclear experimental setups not only lower experimental cost but also ensures higher data quality.

The type of nuclear data experiment involve in this study is the measurement of proton spallation cross sections of tantulum 181. The experiment will be built upon existing data with the assumption that the current data are within close proximity to the actual nuclear properties. The most effective method for finding an optimal experimental setup is to use Monte Carlo particle transport simulations to model the detector environment in a nuclear data experiment across a broad range of configurations. Then, an optimiser will be able to deduce the optimal solution using the simulation result from each of those configurations.

The OpenMC model is able to achieve results within 30-40% of experimental result on a set of Eu-152 callibration data. The optimal experimental setups are sucessfully found when attempting to produce 10,000 counts under the 233.9 keV photopeak, a signature peak from the radioactive product of Ta-181 (p,3n) reaction, whilst satisfying constraints and bounds that arise due to physical limitations and safety concerns. The optimisation process is repeated for activation proton energy across the 5-30 MeV range.

Contents

Chapter 1

Introduction

Nuclear data has many applications in the field of science and engineering, such as the design of nuclear reactor, spacecrafts, and medical devices. However, nuclear data is nowhere near perfect nor complete. Some of the nuclear cross section and gamma data on activated materials are even purely theoretical due to the abundance and compelexity of radiation emitted by its radionuclide products; reading such radiation data can often be challenging.

Researchers are constantly seeking more accurate data through experiments. In order to achieve high quality results efficiently, optimal experimental setups are required. The design of an optimal setup however is not an easy task, as there are many constraints when it comes to actual nuclear data experiments: one of which being time. The purpose of optimising experimental time has a strong financial incentive, as the availablity of experimental facilities comes with a cost. Another constraint would be the radiation dose of the experiment, as high radiation dose not only poses safety concerns but could also incur further costs in radiation shielding procedures and equipment damage.

The interested material and reaction type in this research is tantulum metal under proton irradiation. Tantulum is a very durable metal with excellent heat and mechanical properties, and it is widely used in advanced electronics and aerospace industries (Buckman 2000). When these technologies are exposed to environments with high energy proton radiation, such as outer space or a proton sources like reactor external source or proton therapy machines, having precise knowledge of properties like proton-induced reaction cross sections becomes critically important.

The goal of this research is to produce an accurate simulation model of a HPGe detector using OpenMC and the activated element in study. After which, certain parameters of the experimental setup can be optimised within the model for each reaction route of the activated element, with the goal to produce gamma spectrum that has prominent and defined photopeaks which will reveal the cross section of each reaction route, whilst maintaing a reasonable dose and minimising time. This will hopefully provide useful preparations to the actual nuclear data experiment that take place in the future.

Chapter 2

Theory

2.1 Nuclear Data Experiments

Nuclear data experiments tends to obtain information on the properties of atomic nuclei and their interactions such as reaction cross sections, reaction products etc. In this research, the proton activated tantulum in the form of a very thin foil, which is composed of 99.9% Ta-181, is the main element of interest. The foil will be irradiated by a proton beam with energy in the range of 5-30MeV, inducing proton spallation within the foil and produce a list of radionuclides that emmit gamma rays. This piece of activated foil will then be placed in front of a hyper pure germanium (HPGe) detector, allowing the detector to collect its gamma data.

2.1.1 Proton Spallation

Spallation is a reaction in which a target nucleus is bombarded by very high-energy particles (Ahmed 2015). The incident particle, a proton in this case, collides with the target neucleus, and undergos many possible types of reaction mechanisms: $(p, p)\,(p, n)\,(p, \gamma)\,(p, \alpha)\,(p, t)\,(p, p+n)\,(p, 2n)$... The result of which is the emission of protons, neutrons, photons, alpha particles, and other types of particles, or a combination of them. The current understanding of proton spallation reactions can be found in the IAEA ENDF database.

2.1.2 HPGe Detector

The detector used in this experiment is a hyper pure germanium (HPGe) detector. HPGe detector is a very popular type of gamma detector used in nuclear data exerpiment due to its exceptionally high energy resolution comparing to other types of detector such as a scintillator detector. The HPGe detector is esentially a semiconductor crystal. The crystal resembles a p-n junction system first discovered by Russell Ohl. The germanium crystal is separated into three layers in this system: the lithium doped n-type germanium, the boron doped p-type germanium, and the layer between the two doped regions are known as the p-n junction (Lakatoş 2018). The p-n junction, also known as the depletion layer of the detector, is the active volume of the crystal. The thickness of the depletion layer expands when an electric field is applied across the p-n junction by connecting the crystal to a reversed biased circuit. When an external ionising particle enters the active volume of the germanium crystal, it often collides many times with the electrons within the depletion layer. During each collision, the external ionising particle imparts its own energy to an electron. Due to semiconductor's small band gap between its valence band and conduction band, the electron is easily lifted to the conduction band from the valence band, leaving a hole behind where the electron used to be; this product is known to be an electron-hole pair charge carrier. The creation of each charge carrier induces voltage drop across the reversed bias circuit which can be picked up as a current pulse (Goulding 1966).

Figure 2.1: HPGe detector structure

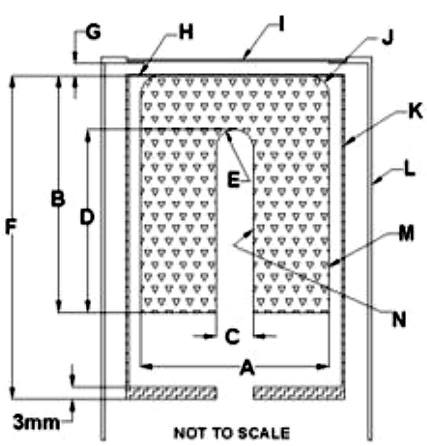

	Dimension [cm]		Dimension [cm]
A	4.93	H	0.003 + 0.003
B	5.29	I	0.05
C	1.19	J	
D	4.58	K	0.08
E		L	0.1
F	9.4	M	0.000003
G	0.3	N	0.00007

The experiment uses the HPGe detector (33-TN20036); Its general structure and dimensions can be found in figure 2.1.

2.1.3 Callibration

The callibration of the detector often uses a common isotope with pronounced and well established photopeaks such as Eu-152. Eu-152 also offers a different advantage which is its wide variety of energy photopeaks

The goal of which is to designate the correct energy value to each energy bin, often by doing a two point callibration on two identified photopeaks. The use of callibration source also provides general information of the detector such as detector resolution and detector efficiency by finding the collected photopeaks' full width half maximum and peak area with respect to energy.

2.2 OpenMC

OpenMC is a Fortran 2008 based Monte Carlo particle transport code developed by the Computational Reactor Physics Group in Massachusetts Institute of Technology (Romano et al. 2015). Though it is much newer than the other existing particle transport codes, it is no less powerful. Like many modern particle transport codes, OpenMC is expected to be scalable in its ability to perform computing intensive simulations, and such is achieved with the help of OpenMP in a shared memory system by instructing compilers to parallelise simulation tasks (Dagum & Menon 1998). This allows OpenMC to work efficiently on modern multi-core and multi-processor systems. For distributed memory system such as a computer cluser, OpenMC uses MPI. OpenMC outshines other particle transport code particularly in its integration with modern programming languages through its python API, this not allows OpenMC codes to be written in a very comprehensible and contemporary format, but it also made it conveninet to access python tools and libraries for high quality geometry visualisation, result analysis, and advanced simulation optimisation. OpenMC is also open source, which means it is widely available for public use. The wide access to this technology should promote developemnt of the code through the collaboration of user's feedbacks and validations.

2.2.1 OpenMC Simulation

In order to run an OpenMC simulation, there are several key components that needs to be included in the directory: material, geomtry, settings, and tallies. Each one specifies a particular aspect of the simulation setup. They are each saved in xml format and can be written using the OpenMC Python API.

OpenMC then simulate the particles based on the setup specification, every generated particle will have its properties tracked along its trajectroy and interactions. A preset number of particles are simulated in a batch, and increasing the number of batches directly reduces the statistical uncertaintities in the simulation result. The type of simulation results is specified by the user, but regardless, it will be saved in a statepoint file in h5 format, which can be extracted into manageable data with the built in python API.

2.2.2 Simulation Statistical Differences

From initial comparison of simualtion data and experimental data, one may find that corresponding photopeaks of each data type will share similar area but not shapes. The reason of such differences have to do with the statistical variance of the detector which a particle transport code fails to take into consideration. The variance observed in pulse height tally within OpenMC's simualtion is likely generated naturally due to the stochastic nature of the monte carlo codes (*OpenMC Documentation - Tallies* n.d.). However, in a real detector setup, there exists more variables that increases the complexity of statistics. For instance, the number of charge carriers produced during the interaction of an iosning particle and the active volume of a semiconductor detector is inherently subjected to statistical fluctuation; such fluctuation which may initially be expected to be directly related to the initial energy of the ionising particle in fact does not follow a simple statistical distribution. This discrepancies between an ideal poission distribution and the actual distribution of in number of charge carrier produced is first studied in (Fano 1947). Another factor lies within the structure of the crystal lattice. The actual crystal quality often is limited by the complexity of the p-n junction which results in phenomenon like charge trapping and poor charge carrier mobility (Devanathan et al. 2006). The translation from the collection of charge carrier to an electrical signal also involves deadtime and electronic noises from the various electronic equipment. All these factors combined makes the actual statistical variance of the experiment to be much larger than simulation results.

2.3 SciPy Optimise - SLSQP

SciPy Optimise (*SciPy v1.14.1 Manual Documentation* n.d.) is a very simple yet useful optimisation module available in python. It offers multiple optimisation methods, which users can select depending on the problem on hand. The SLSQP (Squenstial Least Square Programming) minimise method is particularly well suited to solve smooth nonlinear objective problems with contraints and bounds. The routine is originally implemented by Dieter Kraft (Kraft 1988), who advocates the efficiency of sequential quadratic Programming in solving many complex industrial problems like solving nonlinear problems for local minimums. It is therefore chosen to be the main method used for the optimisation stage of this research.

Chapter 3

Methodology

3.1 Pre Simulation Analysis

3.1.1 Spectrum Analysis

Intrepretation of results in this research are mostly conducted in the form of spectrum analysis. It is crucial to ensure that there are proper spectrum analysis tools before the project begins. There are several key python functions that will be be repeatedly employed in the analysis: **peakfinder**, **background** and **findpeakarea**. Peak finder uses the find peaks function in SciPy Signal, filtering peaks across the spectrum by prominence. The function outputs the energy value of the peak and assumes the peak tails locate around ± 3 keV, a subfunction then finds the nearest bins from those two respective values. The background function (not to be confused with the background spectrum obtained from collecting gamma data without the radiation source) finds the average of the two intensity values at the peak edges. The findpeakarea function then sum up all the bins between the peak edges after the subtraction of background function.

3.1.2 Energy Callibration

$$m = \frac{E_{peak1} - E_{peak2}}{bin_{peak1} - bin_{peak2}} \tag{3.1}$$

$$b = E_{peak2} - m \cdot bin_{peak2} \tag{3.2}$$

$$new\ energy\ bins = m(no.\ of\ \ bins) + b \tag{3.3}$$

The energy callibration will be performed using an Eu-152 and a Ba-133 source. Before callibration, the gamma source data of these radionuclides are obtained from the IAEA radionuclide database (IAEA n.d.b). Two photopeaks with distinctive high amplitude are selected manually. Energy callibration is performed on 900 seconds of gamma spectrum collected by the HPGe detector with each source. Using scipy findpeak, the energy bin values corresponding to the most prominant peaks are located. They are then manually matched with the two photopeaks selected beforehand. Using equation 3.1, 3.2, 3.3. The new energy bins will be allocated with the callibrated energy level.

3.1.3 Detector Resolution

$$R = \frac{FWHM(E_{peaks})}{E_{peaks}} \tag{3.4}$$

Detector resolution can best be found by using Eu-152, as it emits a long list of gamma radiation that spans cross a wide range of energy. A function **FWHM** is written to obtain the full width half mamximum of a photopeak, which takes the spectrum data and given peak edges as inputs; it outputs the fullwdith half maximum by finding where the peak curve intersects with a horizontal line at the half length between peak max and background value. FWHM is applied on all prominent peaks found using **findpeaks** across a spectrum. The resulting FWHM over energy graph will allow us to plot the resolution curve of the detector. 3.4 (Drissi El-Bouzaidi et al. 2023). FWHM(E) will be useful later on in the post simulation section in the attempt to replicate detector behvaiour in monte carlo simulation.

3.1.4 Detector Efficiency

$$\epsilon_{abs} = \frac{N_{count}}{N_{source}} \tag{3.5}$$

$$\epsilon(E) = \frac{N_{peakcount}(Epeak)}{N_{source}} \tag{3.6}$$

We will find detector efficiency in the form of total efficiency 3.5 (Tekin & Mesbahi 2015) and an energy efficiency curve 3.6, just to introduce another parameter for future comparisons on the experimental to the simulation detector performance.

3.1.5 Background processing

Collecting a background for elimination purpose is a standard procedue to separate the radiation infromation of interest from the ones caused by earth's background radiation and other potential contamination in the labroatory enviornment. The background will be subtracted from the experimental data after adjustments to the counts are made for any differences in data collection time. This is important as monte carlo simulation by default will not include the background radiation of our laboratory environment.

3.2 OpenMC Simulation

The simulation involved in this research utilises v0.14.1-dev of OpenMC operating on macOS. In the initial stage of simulation development, the first simualtion will attempt to recreate the detector setup at the callibration phase involving the use of Eu-152 source. Following that, more isotopes can be used to callibrate and confirm the accuracy in detector performance.

3.2.1 Material

Figure 3.1: OpenMC simulation material label

The material information used within this experiment will be found in the material compendium (Laboratory 2021). The cross section data will be extracted from the official ENDF/B-VII.1 library.

3.2.2 Geometry

The simulation will attempt to replicate the HPGe detector by following the detector strcutural dimensions and materials given in figure 2.1. It must be noted that some information on detector structure is not given such as the position of the inner alumnium layer, but such details shouldnt have any significant impact to the gamma data collected by the HPGe detector. The resulting geomtry of the detector is placed in an openmc universe wich also encompasses two pieces of lead shields adjacent to both sides of the detector's active volume. The final resulting geomtry is visualised using the in built plot function of openMC (figure3.2,3.1).

Note that, the source will not typically show up as part of OpenMc geometry, as it is a point

Figure 3.2: OpenMC simulation geometry visualised

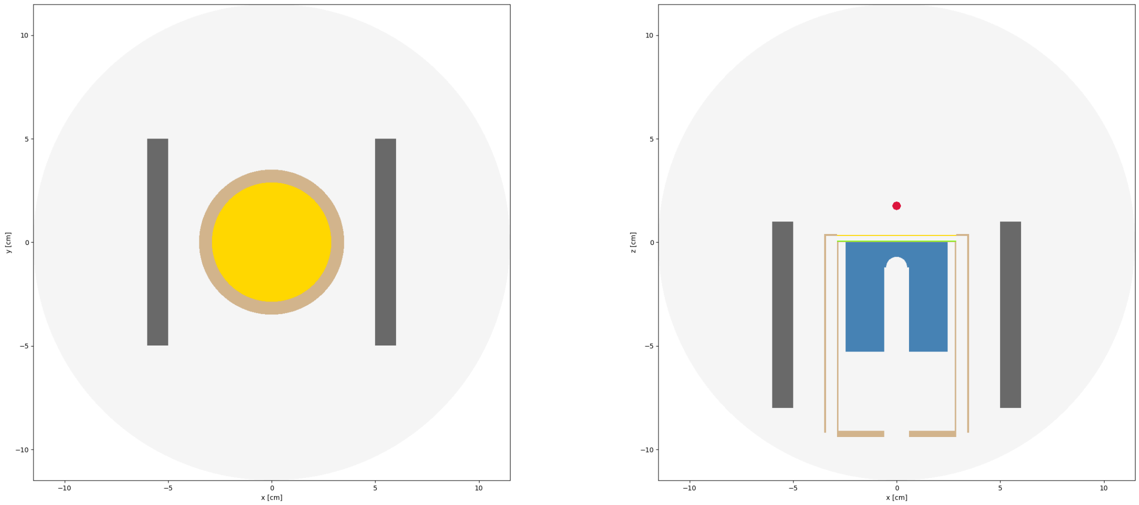

Figure 3.3: A cross sectional visualisation of the experimental setup in the XY plane (left) and XZ plane (right).

source in every part of this research. Its appearence is soleley for visualisation purpose.

3.2.3 Settings

The simulation will use an isotropic point source placed at the same distance away from the detector endcap as in the laboratory experiment. The energy profile corresponding to the isotope in study (eu-152 in the first callibration stage) is extracted from the radionucldie gamma decay database IAEA (n.d.*b*). The source strength is calculated by finding the source activity from the laboratory experiment multiplied by the total gamma decay probability and the time it took to collect the spectrum.

3.2.4 Tally

The interested tally type of this simulation will be the pulse height tally within the germanium cell. This should produce results equivalent to the signal pulse heights of an actual HPGe detector.

3.3 Post Simulation Processing

3.3.1 Gaussian Energy Broadening

To callibrate the detector's statistical variance involves two main steps - finding the actual detector resolution curve, and apply gaussian broadening to the simulation results. The first step should have been partially performed during the pre simulation step on the experimental data, where the full width half maximum of most prominent peaks are found. Next, a resolution curve is fitted to that set of data using the function in equation 3.7.

$$FWHM(E) = a + b\sqrt{E + cE^2} \tag{3.7}$$

The fit should provide the parameter a, b, and c which will be used to adjust the variance of the simulation data. Each simulation data which is a count at an energy value will will be reevaluated in a process given in equation 3.8.

$$E_{GEB} = E + \frac{FWHM}{2\sqrt{ln2}} erf^{-1}(X) \tag{3.8}$$

The actual way to broaden the spectrum peaks is contained within a single function **broaden_spectrum**: it takes the parameter a, b, c and original simulation spetrum as the input. Then, it applies the gaussian function (equation 3.9) on to the original simulation spectrum.

$$\sigma = \frac{a + b * \sqrt{E + c * E^2}}{2 * \sqrt{2 \cdot ln(2)}} \tag{3.9}$$

3.4 Energy Profile of a Spallation Proton Source

The energy profile of the spallation proton source displays a list of gamma energy and their relative intensity per disintegration. Three steps are needed to achieve the energy profile: find $\frac{R}{\sigma}$ (number of reactions / cross section) using experiment setup parameters; find the cross sections of all possible reactions in the target nuclide and multiplying to $\frac{R}{\sigma}$ to the number of reaction products; finally, extract the gamma decay data of each of those reaction products and use bateman's equation to find the number of decay that have taken place within a custom selected time window, which will allow us to find the relative intenesity of each gamma.

3.4.1 $\frac{R}{\sigma}$ from Experiment Parameters

The first step is to find the variable known as $\frac{R}{\sigma}$. This number depends entirely on parameters that can be found directly from the proton irradiation experiment setup: beam current, irradiation time, and the target foil properties like its density, thickness, and amu. The equation of $\frac{R}{\sigma}$ (equation 3.13) is derived below:

$$N = \frac{\rho N_A}{m} \tag{3.10}$$

$$n = \frac{I}{vAe} \tag{3.11}$$

$$V = Ax \tag{3.12}$$

$$\begin{aligned} R &= nvNV\sigma T \\ R &= \frac{NITx}{e} \cdot \sigma \\ \frac{R}{\sigma} &= \frac{NITx}{e} \end{aligned} \tag{3.13}$$

Table 3.1: Variables of proton spallation source calculation

symbol		symbol		symbol	
A	Beam cross sectional area	n	Number density of beam	V	Target Volume
c	Speed of light	N	Number density of target	x	Target thickness
e	Elementary charge	N_A	Avogadro's number	Φ	Beam flux
E_0	Rest energy of proton	p	Momentum of proton	ρ	atomic density of target
E_k	Kinetic energy of proton	R	Number of Reactions	σ	Cross section of target reaction
I	Beam current	T	Irradiation time		
m	Atomic mass of target	v	Speed of protons		

3.4.2 Target Reaction Cross Section

The cross sections of all possible routes of proton spallation (p,) within the range of 5-30MeV are extracted from (IAEA n.d.a); They are combined into a csv file, where the columns are reaction products + routes, and rows are distinct proton energy in the interested range. As σ and $\frac{R}{\sigma}$ are now found, we will be able to deduce how many times each of (p,) reactions have taken place in the irradiation experiment, by extension, we have found the number of each reaction products that have been produced from the proton irradiation.

$$\frac{R}{\sigma_{(p,)}} \cdot \sigma_{(p,)} = R_{(p,)} = N_{1,(p,)}(0) \tag{3.14}$$

3.4.3 Gamma decay

The gamma decay data for every radioactive (p,) product nuclides and daughter nuclides are extracted from (IAEA n.d.b); they are saved in the format of csv files with the following columns: gamma energy, intensity, half-life. (for those with radioactive daughter nuclides, there will also be a daughter nuclide decay probability and daughter nuclide half-life). For each type of gamma decay across every (p,) product nuclides, we can compute the number of decay that will take place within a custom time window by using the bateman's equation and the $N_{1,(p,)}(0)$ found for each reaction product in the previous subsection. This will then be multiplied by the intensity per disintegration column and saved as the actual intensity column.

$$\begin{aligned}
N_n(t) &= N_1(0) \cdot (\prod_{i=1}^{n-1} \lambda_i) \cdot \sum_{i=1}^{n} \frac{e^{-\lambda_i t}}{\prod_{j=1, j\neq i}^{n}(\lambda_j - \lambda_i)} \\
N_1(t) &= N_1(0) \cdot e^{-\lambda_1 t} \\
N_2(t) &= N_1(0) \cdot \frac{\lambda_1}{\lambda_2 - \lambda_1} \cdot (e^{-\lambda_1 t} - e^{-\lambda_2 t})
\end{aligned} \tag{3.15}$$

Equation 3.15 is the bateman equation written in the form of the first and second generation nuclides. The number of a nuclide type at a given time can give us a hint of how many decay has taken place in a particular time window (equation 3.16)

$$\begin{aligned} First\ generation\ decay &= N_1(t_i) - N_1(t_f) \\ Second\ generation\ decay &= First\ generation\ decay - (N_2(t_f) - N_2(t_i)) \end{aligned} \tag{3.16}$$

After the total number of decay is found for each gamma energy, the columns are vertically concatenated and normalised into the full gamma energy profile as a new column **intensity_real**. This fixed source profile can be seen as the average gamma emission within a certain time window of the activated foil during the collection of radiation data.

3.5 Optimisation

3.5.1 Pre-Optimisation

Figure 3.4: Experiment parameters to be optimised

	Variable	[unit]
I	Source Beam Current	[μA]
x_{foil}	Foil Distance	[cm]
T_{irr}	Irradiation Time	[s]
E_+	Source Proton Energy	[MeV]
t_i	Foil Cooling Time	[s]
t_{exp}	Experiment Collection Time	[s]

Before any optimisation can be performed, it is necessary to create a function **foilprocess** that will streamline every steps between the input parameters and the output of peak area. Given a set of parameters, that function will calculate the gamma profile and activity of the foil as section 3.4. The result of which is the OpenMC source definition and will subsequently be used to run a simulation of a germanium detector collecting gamma data from such source definition as the foil. Finally, the resulting statepoint file will be extracted and analysed using **peakfinder** and **peakarea**, where the peak area of the preselected peak energy can be calculated. The selection of peak energies will be done by finding the energy level with the highest intensitiy for each reaction route. The optimisation process can then loop through each of those interested peak energy to discover the ideal parameters setup as a means to emphasise on peak energies that are representative to each reaction route.

3.5.2 Objective

The optimisation objective is to be able to collect a significant number of counts under minimal time as an effort to lower experimental cost. A new variable $T_{\sum}$ is created; it is the sum of irradiation time, cooling time, and collection time. The objective function of this optimisation problem will be the definition of $T_{\sum}$ as seen in equation 3.17.

$$T_{\sum} = T_{irr} + t_i + t_{exp} \tag{3.17}$$

3.5.3 Constraints

The measurement of counts using a detector follows a poisson distribution of statistical distribution. Therefore, the variance of the data would be equal to the total number of counts $\sigma^2 = N$. Hence, the relative error is $N^{-0.5}$. If we follow a rule of thumb of keeping the results within ±1% error, a target count of 10^4 is required for the interested peak area. This target count can be written as an equality constraint for the optimisation problem as equation 3.18.

$$
\begin{aligned}
x &= -peak\ area_{goal} + peak\ area \\
x &= -10^4 + peak\ area \\
x &= 0
\end{aligned}
\tag{3.18}
$$

Another constraint that needs to be considered is the radioactivity of the activated foil. If the foil becomes too activated, it becomes a potential hazard to the scientist who will be handling the foil in close proximity. For that reason, the dose rate of the foil should not exceed 50mSV/hr during the time of the data collection. The maximum dose is therefore computed by multiplying the foil dose rate and the time it takes for data collection (equation 3.19).

$$dose_{max} = (50\frac{mSv}{hr}) \cdot t_{exp} \tag{3.19}$$

Since the activity of the foil should be equal or less than the maximum dose. This condition will be an inequality constraint written as equation 3.20.

$$
\begin{aligned}
x &= dose_{max} - dose_{foil} \\
x &\geq 0
\end{aligned}
\tag{3.20}
$$

3.5.4 Bounds

Parameter bounds are physical limitations of the experiment setup or a realistic time limitations for the experiment. As an exmaple, the foil cooling time, seen in figure 3.5, has a bound of 120 - 864000 seconds. The lower limit ensures that there is adequate time to transfer the foil from its irradiation setup to the gamma detector setup; the upper limit is 10 days, which is the upper limit of the entire experiment duration (a foil can be left in the laboratory to await for gamma data collection on a different day, as long as it is optimal).

Figure 3.5: Experiment parameters bounds

	Variable	[unit]	Bounds
I	Source Beam Current	[μA]	0.001 - 10
x_{foil}	Foil Distance	[cm]	0.1 - 20
T_{irr}	Irradiation Time	[s]	30 - 3600
E_+	Source Proton Energy	[MeV]	5 - 30
t_i	Foil Cooling Time	[s]	120 - 864000
t_{exp}	Experiment Collection Time	[s]	100 - 86400

Chapter 4

Results and Discussion

4.1 Callibration

4.1.1 Pre-simulation

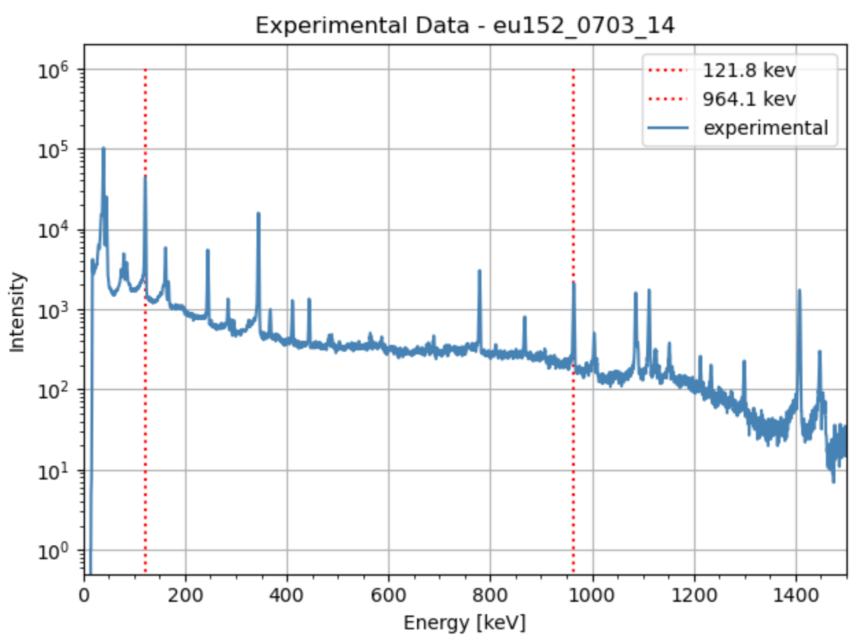

Figure 4.1: Callibrated gamma spectrum of the Eu-152 source

Experimental data using the HPGe detector and a callibration source was collected in an experiment dating back to two years ago. The experiment conducted with a Eu-152 callibration source; background data is also available for that experiment. The Eu-152 data were subtracted by the background and plotted; the energy axis is subsequently callibrated using the 121.8keV and 981keV photopeaks with the two point technique discussed previously. The resulting spectrum is figure 4.1.

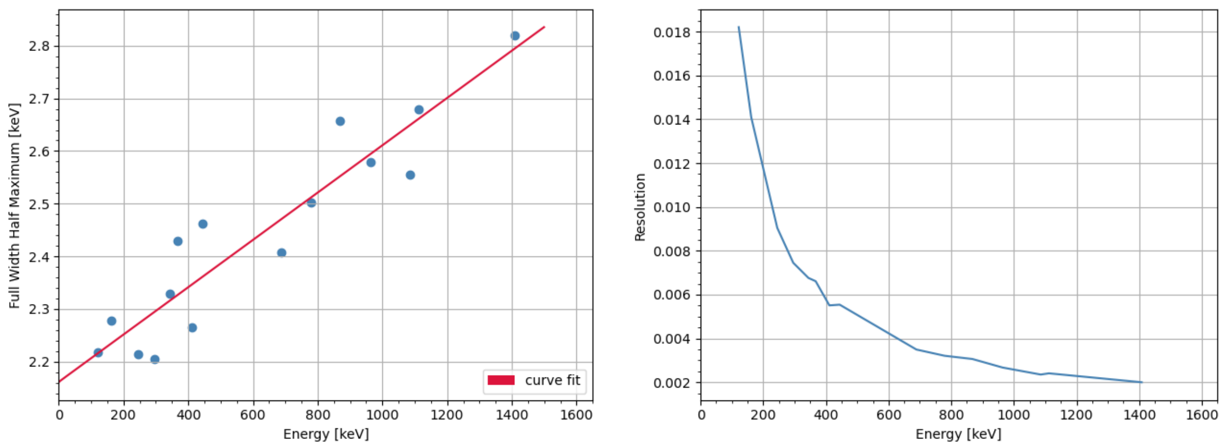

Figure 4.2: The curve fit of photopeaks fwhm from the Eu-152 spectrum (left), the resolution curve of the detector found using fwhm the fwhm graph (right)

The resolution of the HPGe detector is assessed using the above Eu-152 data. The FWHM increases linearly along the energy axis and lies between 2.2-2.6 keV from 0-1000keV. The resolution data behaves as expectedly, as it tends to decrease from low energy range to high energy range, with FWHM in the range of 1-2.5keV. For confirmation, similar behaviours of HPGe resolution can be observed in (I. Hossain 2012). Our HPGe seems to have a relatively lower resolution than average. The resolution curve fit yields $fwhm = 1.288357 + (0.040774 * \sqrt{energy + (-0.000195) * energy^2})$ The parameters a, b ,and c are therefore 1.288357, 0.040774, -0.000195 respectively.

4.1.2 Simulation of Callibration Source

The experimental data of Eu-152 callibration source is compared with the results from openMC simulation. The spectrums are fairly agreeable even prior processed: photopeaks are found at expected location, and intensities are generally in the right magnitude with similar changes along the energy axis. The differences in peak area is significant. As seen in figure 4.3 (right) The experimental peak area of the 970 keV peak is $3.007 \cdot 10^4$ comparing to $3.913 \cdot 10^4$

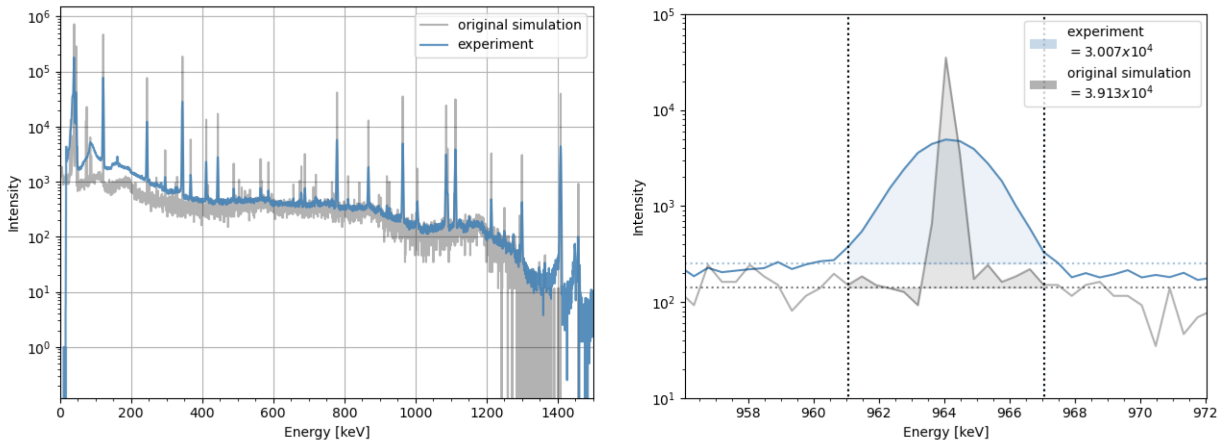

Figure 4.3: Comparison of experimental data and original simulation data - Eu-152 Full Spectrum (left), 970keV photopeak surrounding region (right)

of the simulation peak area, which is roughly +30% difference. The peak base is also slightly different: $2.521 \cdot 10^2$ and $1.410 \cdot 10^2$ for experimental and simulation data respectively. This differences in baseline of -40% seems to occur uniformly across the spectrum.

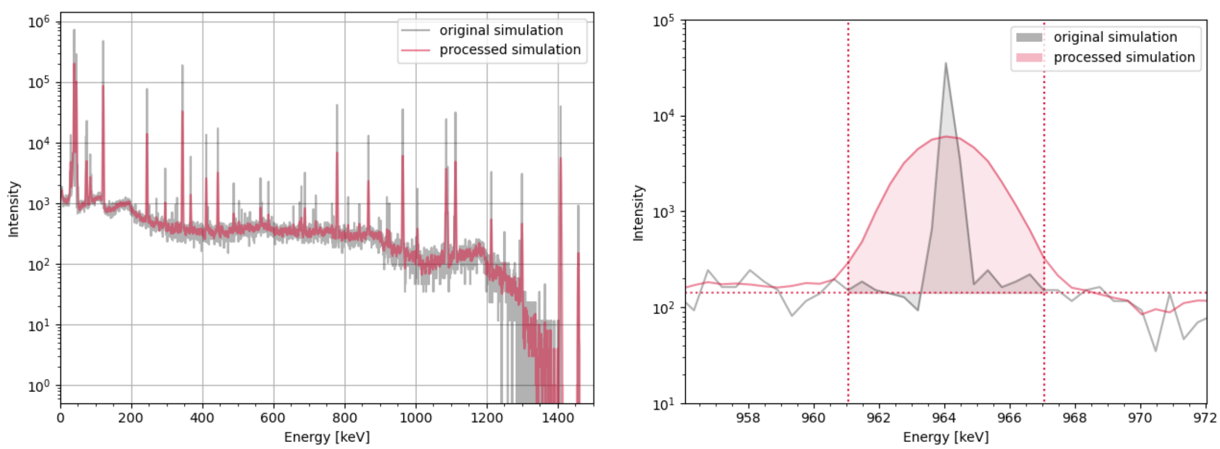

Figure 4.4: Comparison of original simulation data and processed simulation data - Eu-152 Full Spectrum (left), 970keV photopeak surrounding region (right)

After applying gaussian broadening onto the original simulation data, the peak shapes appear to resemble the ones found in an actual spectrum. Nevertheless, it can be seen that the peak still retains its integral properties such as the peak baseline and area.

Final comparison on the experimental data versus processed data clearly shows more agreeing results. Previous discreapncies of photopeaks intensities have mostly been eliminated.

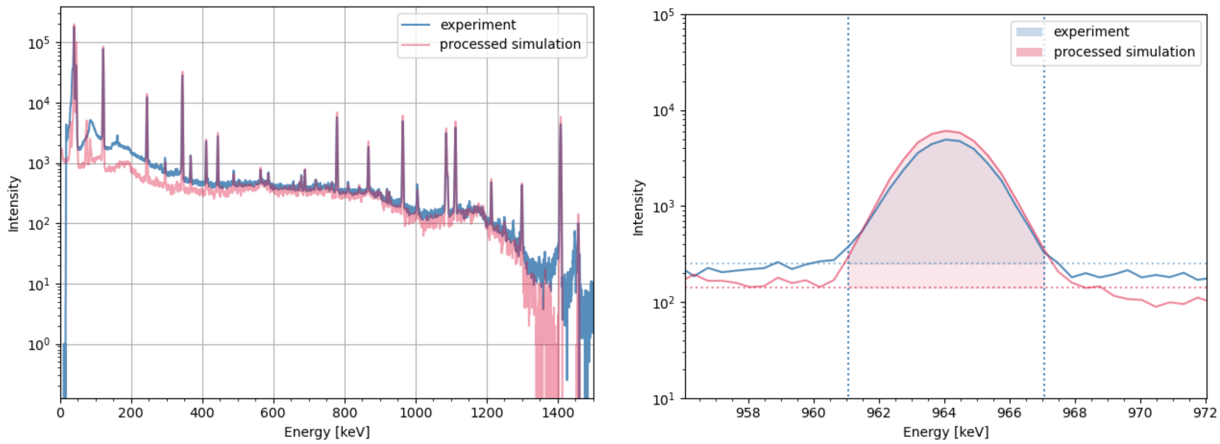

Figure 4.5: Comparison of Experimental Data Processed Simulation Data - Eu-152 Full Spectrum (left), 970keV photopeak surrounding region (right)

The actual differences between experimental data and simulation data now become more pronounced. Most differences occur in the lower energy region where not only the intensities of the baseline are off by a factor of 2, there are also peaks that are absent in the simulation data.

Efforts have been made to account for the differences in results. This includes deducting background, gaussian broadening of the simulation results and further modification of the simulation model by adding the leadshield surroudngin the detector. These steps have in fact increase the the resmeblences of the spectrums, but there might still be certain underlying factros for which are not yet account. This is especially challenging however since the actual collection of the experimental data were performed years ago with potentially missing or erronous data on source properties or source distance.

4.2 Foil source definition

```
energy_p,ta180_np,w181_n,w180_2n,w179_3n,hf177_na,ta178_2nd,hf176_2na,hf175_3na,
5.00E+06,0.0000E+0,2.2915E-4,0.0000E+0,0.0000E+0,3.0851E-18,0.0000E+0,0.0000E+0,
6.00E+06,0.0000E+0,2.4842E-3,0.0000E+0,0.0000E+0,1.2310E-14,0.0000E+0,0.0000E+0,
7.00E+06,0.0000E+0,1.4540E-2,0.0000E+0,0.0000E+0,4.1075E-12,0.0000E+0,0.0000E+0,
8.00E+06,6.5609E-18,5.2282E-2,5.8987E-4,0.0000E+0,2.8939E-10,0.0000E+0,0.0000E+0
9.00E+06,1.9785E-12,8.7912E-2,4.1569E-2,0.0000E+0,3.0678E-9,0.0000E+0,0.0000E+0,
1.00E+07,5.9467E-10,9.5667E-2,1.3965E-1,0.0000E+0,2.4129E-8,0.0000E+0,0.0000E+0,
1.10E+07,3.0209E-8,8.8603E-2,2.6487E-1,0.0000E+0,1.4538E-7,0.0000E+0,6.7062E-18,
1.20E+07,6.2306E-7,0.0000E+0,3.9615E-1,0.0000E+0,6.9899E-7,0.0000E+0,4.8890E-14,
1.30E+07,6.3313E-6,6.6222E-2,5.2345E-1,0.0000E+0,2.5710E-6,0.0000E+0,6.9879E-12,
1.40E+07,3.6019E-5,5.6370E-2,6.4163E-1,0.0000E+0,7.8936E-6,0.0000E+0,3.0804E-10,
1.50E+07,1.4488E-4,4.8941E-2,7.4759E-1,0.0000E+0,2.2937E-5,0.0000E+0,5.5900E-9,0
1.60E+07,4.7468E-4,4.3954E-2,8.3946E-1,0.0000E+0,6.4761E-5,0.0000E+0,5.2148E-8,0
1.70E+07,1.3016E-3,4.0911E-2,9.1072E-1,6.3722E-3,1.7167E-4,0.0000E+0,2.8356E-7,0
1.80E+07,2.9861E-3,3.9195E-2,8.9571E-1,8.6435E-2,4.2929E-4,0.0000E+0,8.5051E-7,0
1.90E+07,5.8448E-3,3.8224E-2,7.7742E-1,2.5778E-1,1.1290E-3,0.0000E+0,2.4094E-6,0
2.00E+07,1.0518E-2,3.7593E-2,6.1270E-1,4.5616E-1,4.0097E-3,0.0000E+0,7.4635E-6,1
2.20E+07,2.4466E-2,3.6550E-2,3.4725E-1,7.8700E-1,9.6273E-3,0.0000E+0,6.1413E-5,1
2.40E+07,4.4104E-2,3.5336E-2,2.0580E-1,9.9668E-1,6.5098E-3,5.2201E-12,2.9440E-4,
2.60E+07,6.6594E-2,3.3838E-2,1.3939E-1,1.0748E+0,7.3946E-3,4.4458E-8,9.6619E-4,1
2.80E+07,8.8922E-2,0.0000E+0,1.1073E-1,9.9174E-1,7.9819E-3,5.7188E-6,2.2156E-3,2
3.00E+07,1.0909E-1,3.0734E-2,9.7673E-2,7.8176E-1,8.0339E-3,1.2146E-4,3.9839E-3,2
```

Figure 4.6: Ta-181 (p,) reactions cross section file format

Using the resources available on TENDL-2023 cross sectional database (IAEA n.d. *a*), a source definiton of the proton activated tantulum foil can be constructed. The resulting source definition is made up of 29 different reactions that can yield various isotopes with mass number in the range of 173-181. The cross sectional data is available for energy in the range of 5-30MeV, and it is in the form of a csv file.

Figure 4.7: W-179 Processed Gamma Data

```
energy,intensity,half_life,fraction_m,half_life_m
30.7,18,2223,0,0
133.9,0.1062,2223,0,0
9.424,28.87470827,2223,0,0
56.28,22.39764477,2223,0,0
57.535,39.04749786,2223,0,0
65.315,12.91799455,2223,0,0
66.067,16.40585308,2223,0,0
66.981,3.487858529,2223,0,0
9.114,20.222748,57433605.27,1,2223
54.608,12.61950366,57433605.27,1,2223
55.786,22.08523567,57433605.27,1,2223
63.333,7.286077872,57433605.27,1,2223
64.057,9.231460664,57433605.27,1,2223
64.935,1.945382792,57433605.27,1,2223
```

Gamma data on the tantulum proton spalltion products are each stored separately in a csv file. An example gamma file of W-179, a radioactive product from Ta-181 (p,3n) reaction, can be seen in figure 4.7. Product nuclides with further radioactive daughter nulcides have 0 under **fraction_m** and **half_life_m**, and product nuclides that are stable will have 0 written under every column.

	energy	decay	intensity_real	intensity
0	0.000	0.000000e+00	0.000000e+00	0.000000
1	6.240	2.870116e+05	3.025005e-06	1.030000
2	8.810	5.528513e-08	5.826865e-19	25.100000
3	9.114	1.047346e+09	1.103867e-02	252.517012
4	9.424	1.749882e+10	1.844317e-01	71.006057
..	...	...	...	...
91	1496.010	0.000000e+00	0.000000e+00	0.268800
92	1513.630	0.000000e+00	0.000000e+00	0.004608
93	1561.300	0.000000e+00	0.000000e+00	0.010560
94	1678.810	0.000000e+00	0.000000e+00	0.003696
95	1772.000	0.000000e+00	0.000000e+00	0.000000

Figure 4.8: Source energy profile example of parameters set: (beam_current = 9e-6 A, cooling_time = 10000 s, counting_time = 1000 s, distance_foil = 5 cm, irradiation_time = 3600s), where foil is activated by 20MeV protons

To demonstrate how the above information is translated to an openmc source definition, a set of initial parameter (beam_current = 9e-6 A, cooling_time = 10000 s, counting_time = 1000 s, distance_foil = 5 cm, irradiation_time = 3600s) is used to calculate the source definition. The resulting gamma source profile can be seen in figure 4.8 with a total source activity of $9.49 \cdot 10^{11}$ disintegration within the duration of gamma collection.

4.3 Optimisation

The first optimisation problem will be to optimise for the ideal parameters in the search of Ta-181 (p,2n) reaction cross section. The product of such reaction is W-180, which has various prominent photopeaks from which to choose. The 233.9 keV photopeak is selected as the representative photopeak due to its high intensity and distinction from other photopeaks.

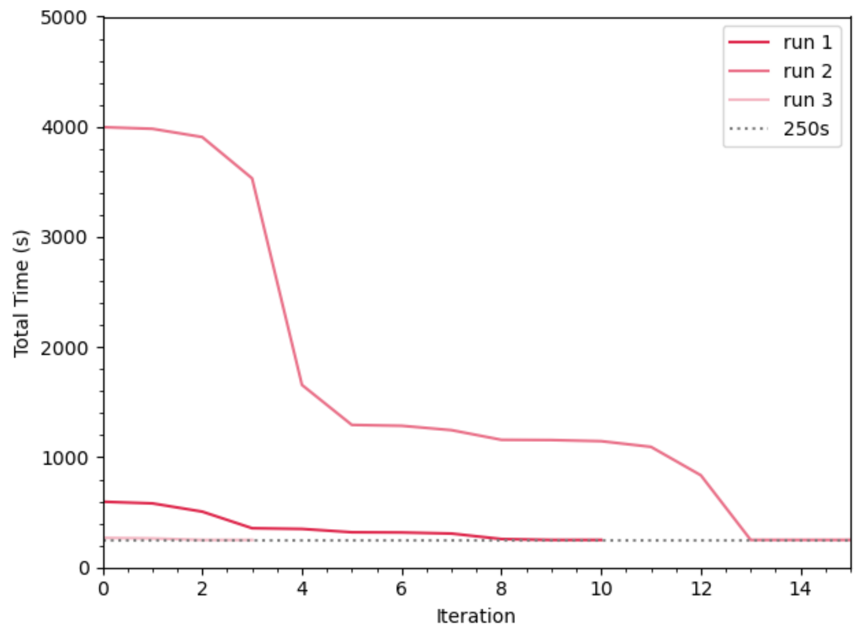

Figure 4.9: Ta-181 (p,2n)(233.9keV) - Optimisation iteration progression of 3 sets of parameters.

The behaviour of the SLSQP optimsiser is recorded for the optimisation problem on 20 keV proton energy in search of the 233.9 keV photopeak (figure 4.9). The optimiser converges at a local minimum of 250 seconds, and it is confirmed by inputting three distinct sets of parameters. The unanimous end solution for this optising problem is (beam current = $4.17\mu A$, cooling time = 120s, counting time = 100s, distance = 5cm, irradiation time = 30s). Though it isnt entirely certain whether this is the globally ideal parameter sets, it does satisfy all the constraints that it has been given: The activated foil emits 0.062 μSv throughout the entire detector collection window, which is well below the radiation limit; it will also produce a 233.9keV photopeak with a peak area of 10000 counts.

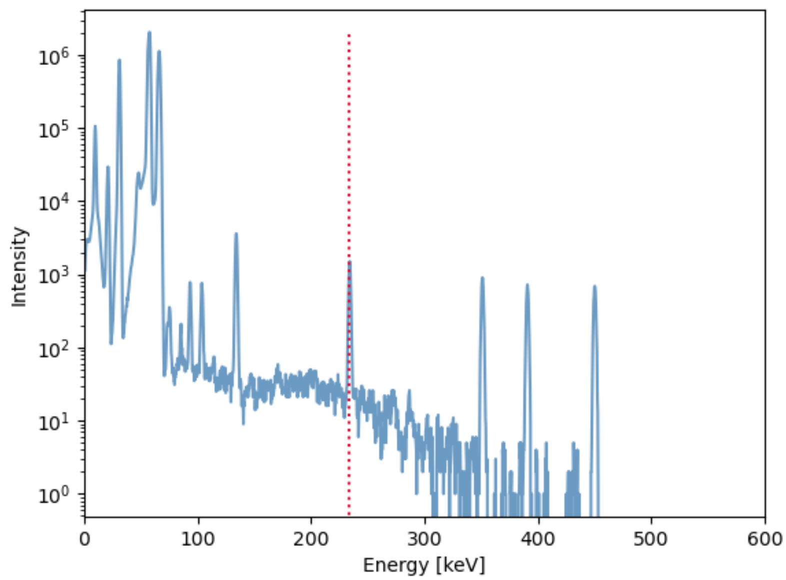

Figure 4.10: Ta-181 (p,2n)(233.9keV) - The gamma spectrum produced by the optimised parameter set (4.17μA, 120s, 100s, 5cm, 30s) with the 233.9keV peak highligted

The end solution of using other proton energy as a foil activation source is listed on table (4.1). By tracking the optimiser iterations, it seems that the optimiser is reluctant to change the distance parameter; The distance 5cm therefore remains the same throughout. For low proton energy (¡7 MeV), 5cm no longer suffice, given all other coniditions are held the same. The only way is to decrease the distance between the detector and source. Decreasing the distance to the lower limit will be able to produce valid parameters when beam current, counting time, and irradiation time are at/near their upper limit. The validity of these result will require confirmation from actual experiments.

Table 4.1: Ta-181 (p,2n)(233.9keV) - Optimisation Result for various proton energy

Energy (MeV)	Beam Current (μA)	Cooling Time (s)	Counting Time (s)	Distance (m)	Irradiation Time (s)
20	4.171	120	100	5	30
19	6.809	120	100	5	30
18	10	120	100	5	40.86
17	10	120	100	5	69.27
16	10	120	127.3	5	127.5
15	10	120	218.1	5	218.4
14	10	120	441.7	5	441.3
13	10	120	1149	5	1102
12	10	120	4064	5	3600
11	0	0	0	0	0
10	10	120	4639	5	3600
9	10	120	5048	5	3600
8	10	120	8489	5	3600
7	10	120	30550	5	3600

Chapter 5

Conclusion

The goal of this study is to come up with an optimisation routine that searches for the optimal experimental setups in the measurement of proton activated tantulum reaction cross sections using a hyper pure germanium detector. The process is sucessful: To replicate experimental results efficiently, a simulation model is made in OpenMC, which is able to achieve results within 30-40% of experimental callibration data. The proton activated element is also successfully implemented into the simulation model through a custom source definition calculated using existing gamma and cross section data. Optimisation results are achieved: The 233.9 keV photopeak is used as an example peak of interest, which represents the Ta-181 (p,3n) reaction. The optimal setup in producing the target net count for such peak is found for activation proton energy between 5-30 MeV (table 4.1).

Bibliography

Ahmed, S. N. (2015), 2 - Interaction of radiation with matter, *in* S. N. Ahmed, ed., 'Physics and Engineering of Radiation Detection (Second Edition)', Elsevier, pp. 65–155.
URL: *https://www.sciencedirect.com/science/article/pii/B9780128013632000024*

Buckman, R. W. (2000), 'New applications for tantalum and tantalum alloys', *JOM* **52**(3), 40–41.
URL: *https://doi.org/10.1007/s11837-000-0100-6*

Dagum, L. & Menon, R. (1998), 'OpenMP: an industry standard API for shared-memory programming', *IEEE Computational Science and Engineering* **5**(1), 46–55. Conference Name: IEEE Computational Science and Engineering.
URL: *https://ieeexplore.ieee.org/abstract/document/660313*

Devanathan, R., Corrales, L. R., Gao, F. & Weber, W. J. (2006), 'Signal variance in gamma-ray detectors—A review', *Nuclear Instruments and Methods in Physics Research Section A: Accelerators, Spectrometers, Detectors and Associated Equipment* **565**(2), 637–649.
URL: *https://www.sciencedirect.com/science/article/pii/S0168900206009089*

Drissi El-Bouzaidi, M., El Bardouni, T., El Hajjaji, O., Idrissi, A., Chham, E., Pérez, A. M. & Mira, M. (2023), 'Simulation of a NaI(Tl) detector model using OpenMC modified on code source and validation using experimental and simulated results', *Radiation Physics and Chemistry* **206**, 110777.
URL: *https://linkinghub.elsevier.com/retrieve/pii/S0969806X23000221*

Fano, U. (1947), 'Ionization Yield of Radiations. II. The Fluctuations of the Number of Ions',

Physical Review **72**(1), 26–29. Publisher: American Physical Society.
URL: *https://link.aps.org/doi/10.1103/PhysRev.72.26*

Goulding, F. S. (1966), 'Semiconductor detectors for nuclear spectrometry, I', *Nuclear Instruments and Methods* **43**(1), 1–54.
URL: *https://www.sciencedirect.com/science/article/pii/0029554X66905313*

I. Hossain (2012), 'Efficiency and resolution of HPGe and NaI(Tl) detectors using gamma-ray spectroscopy', *Scientific Research and Essays* **7**(1).

IAEA (n.d.*a*), 'ENDF: Evaluated Nuclear Data File'.
URL: *https://www-nds.iaea.org/exfor/endf.htm*

IAEA (n.d.*b*), 'Livechart - Table of Nuclides - Nuclear structure and decay data'.
URL: *https://www-nds.iaea.org/relnsd/vcharthtml/VChartHTML.html*

Kraft, D. (1988), 'A software package for sequential quadratic programming', *Deutsche Forschungs- und Versuchsanstalt fur Luft- und Raumfahrt* .

Laboratory, P. N. N. (2021), *Compendium of Material Composition Data for Radiation Transport Modeling*, US Department of Homeland Security. 200-DMAMC-128170 PNNL-15870, Rev. 2.

Lakatoş, E. S. (2018), '60 Years from the Invention of the Integrated Circuits'.

OpenMC Documentation - Tallies (n.d.).
URL: *https://docs.openmc.org/en/v0.14.0/methods/tallies.html*

Romano, P. K., Horelik, N. E., Herman, B. R., Nelson, A. G., Forget, B. & Smith, K. (2015), 'OpenMC: A state-of-the-art Monte Carlo code for research and development', *Annals of Nuclear Energy* **82**, 90–97.
URL: *https://www.sciencedirect.com/science/article/pii/S030645491400379X*

SciPy v1.14.1 Manual Documentation (n.d.).
URL: *https://docs.scipy.org/doc/scipy/*

Tekin, H. O. & Mesbahi, A. (2015), ‘Calculation of Detection Efficiency for the Gamma Detector using MCNPX’, *Acta Physica Polonica A* **128**, B–332.